CHEMICAL PHYSICS

Covalent-like bondings and abnormal formation of ferroelectric structures in binary ionic salts

Yin Dai and Menghao Wu*

In the Mooser-Pearson diagram, binary ionic compoundss form into nonpolar symmetrical structures with high coordination numbers, while wurtzite structures should appear in the covalent region. Their tetrahedral bonding configurations break the inversion symmetry, with polarizations almost unswitchable due to the high barriers of abrupt breaking and reformation of covalent bonds. Here, through first-principles calculations, we find some exceptional cases of highly ionic ferroelectric binary salts such as lithium halides, which may form into wurtzite structures with covalent-like sp^3 bondings, and the origin of these abnormal formations is clarified. Their high polarizations induced by symmetry breaking are switchable, with much smoother switching pathway refrained from abrupt bond breaking due to the long-range feature of Coulomb interactions. These covalent-like ionic bondings do reduce not only their ferroelectric switching barriers but also the phase transition barriers between polar and nonpolar phases, rendering high performance in applications such as nonvolatile memory and energy storage.

INTRODUCTION

In the Mooser-Pearson diagram (*1*) mapping the crystal structures of binary normal valence compounds, tetrahedral structures [wurtzite (WZ) and zinc-blende (ZB)] are located in the covalent zone with low electronegativity difference and low average principal quantum numbers related to high s-p hybridization, e.g., prevalent semiconductors ZnO and AlN with covalent sp^3 bonding configurations breaking the inversion symmetry. They are distinctly separated from the centrosymmetrical structures with higher coordination numbers such as rock salt (RS) or cesium chloride (CsCl) types where the coordination numbers are 6 and 8, respectively, higher than the coordination number of 4 for covalent sp^3 hybridizations These configurations are favored by ionic compounds such as NaCl and CaO, as the Madelung constants can be maximized to minimize the lattice energy.

According to the Philips scale (*2*), the chemical bond in insulators and semiconductors has been divided into a covalent part E_h and an ionic part C, where the ionicity is defined as $f_i = C^2/(C^2 + E_h^2)$ and the critical value of 0.785 marks the idealized boundary between predominantly "covalent" and "ionic" systems (*3*). For those covalent binary compounds with ionicity lower than 0.785, WZ or ZB structure will be favorable in energy, e.g., BN, AlP, and ZnS, with ionicity of 0.256, 0.307, and 0.623, respectively. Although their crystalline polarizations are formed as the covalent sp^3 bonding configurations that break the inversion symmetry, their polarizations are almost unswitchable due to the brittle nature of covalent bonding. For example, the calculated polarization switching barrier for WZ ZnO (*4*, *5*) and AgI (*6*) is both over 0.25 eV/f.u. (format unit), with the abrupt breaking and reformation of Zn—O or Ag—I bonds involved during switching. A later study expands the exploration of ferroelectricity in a series of WZ structures including CuCl, CuBr, CuBr, BeS, MgS, MgSe, MnSe, MnTe, ZnTe, AlP, AlAs, AlSb, GaP, GaAs, GaSb, InP, and InAs (*7*), and the lowest barrier among them (0.17 eV/f.u. for CuCl) still implies a high coercive field. Even if an ultrahigh electric field is applied regardless of energy cost, it may induce electrical breakdown instead of polarization switching in those semiconductors with moderate bandgaps. The coercive field can be reduced by doping and making the systems more ionic, e.g., to 2 to 5 MV/cm in $Al_{1-x}Sc_xN$ (*8*) and $Zn_{1-x}Mg_xO$ (*9*), still two orders of magnitude higher compared with prevalent perovskite ferroelectrics like $BaTiO_3$ (25 kV/cm). Compared with the short-range covalent bondings, ionic interactions span a much longer range in the lattice. If an ionic polar structure can be realized, then the switching barrier may be greatly reduced, and a simple and facile binary ferroelectric material can be obtained for various applications. However, when the ionicity increases above 0.785, the preferable structures such as RS or CsCl types are all nonpolar due to the directionless features of ionic bondings.

Here, we show first-principles evidence that some highly ionic binary compounds such as lithium halides are exceptions, which may form into ferroelectric WZ structures with covalent-like sp^3 bondings. Also contradicting with the general principle in the Mooser-Pearson diagram, the WZ structures are further stabilized in those halides with higher principal quantum numbers, and we clarify these abnormal formations by the analysis of bonding configurations. While these bondings and structures give rise to high polarizations, their high ionicity enables large deformation and ion displacements with low switching barriers. Their ferroelectricity with low-energy consumption in facile materials is highly desirable for nanoelectronic application as nonvolatile random access memories (*10*). Meanwhile, their high ionicity also reduces the barriers of phase transition between polar and nonpolar phases, which may facilitate potential application in energy storage (*11*–*13*).

RESULTS AND DISCUSSION

First, we calculate the energy difference between WZ and RS phases $\Delta E = E(\text{WZ}) - E(\text{RS})$ for a series of common binary compounds and plot the dependence of ΔE on their Philips ionicity (*2*) in

School of Physics and Institute for Quantum Science and Engineering, School of Chemistry and Institute of Theoretical Chemistry, Huazhong University of Science and Technology, Wuhan 430074, China.
*Corresponding author. Email: wmh1987@hust.edu.cn

Fig. 1. It seems that WZ structure is more favorable in the covalent zone with ionicity below the critical value of 0.785, while the RS structure is the ground state for most binary compounds in the ionic zone with ionicity over 0.785 (the boundary is marked by the red line). However, as marked by the purple circle, it is clearly shown that LiCl, LiBr, and LiI are the few exceptions of highly ionic compounds that favor noncentrosymmetric WZ structures, while LiF, MgS, and MgSe are on the edge. Also contradicting with the general principle in the Mooser-Pearson diagram, in Fig. 1, ΔE(LiI) < ΔE(LiBr) < ΔE(LiCl) < ΔE(LiF), so WZ structures seem to be further stabilized with higher average principal quantum numbers. With similar tetrahedral configurations but smaller Madelung constants, the corresponding ZB structures are all higher in energy compared with WZ structures for these ionic systems.

The ion radius (*14*) of the ions in those structures are listed in Table 1. The formation of those ionic WZ structures may be attributed to the small ion radius of Li and Mg cations (60 and 65 pm) compared with anions (181, 195, 216, 184, and 198 pm for Cl^-, Br^-, I^-, S^{2-}, and Se^{2-}), where the repulsion between adjacent anions makes the close packed structures unfavorable. As shown in Fig. 2A, for a RS structure composed of A cations and B anions, the ratio of adjacent B-B distance over adjacent A-B distance should be 1.414, so a considerable repulsion will be induced when $(r_B + r_B):(r_A + r_B) > 1.414$, i.e., $r_B:r_A > 2.42$, where LiCl, LiBr, LiI, MgS, and MgSe are all eligible. In comparison, sodium halides are not within this range given the much larger ion radius of Na cation (95 pm), so RS structures will be favorable without this repulsion. The WZ structures of LiCl, LiBr, and LiI will also be refrained from this repulsion as the distances between two adjacent anions are much prolonged (respectively, 3.88, 4.16, and 4.56 Å for WZ compared with 3.60, 3.90, and 4.26 Å for RS), all larger than $2r_B$. Meanwhile, the distances between two adjacent cation and anion are much reduced (respectively, 2.39, 2.55, and 2.79 Å for WZ compared with 2.54, 2.76, and 3.01 Å for RS), which may enhance the Coulomb attraction between them. As shown by the calculated dependence of the interaction energy between two Cl anions on the interatomic distance in Fig. 2B, the energy induced by Coulomb repulsion between two adjacent Cl ions in WZ LiCl (3.88 Å apart) is 0.25 eV lower compared with RS LiCl (3.60 Å apart), noting that each Cl ion has 12 adjacent Cl ions in RS and WZ LiCl. Meanwhile, the energy induced by Coulomb attraction (see Fig. 2C) between adjacent Li and Cl ions in WZ LiCl (2.39 Å apart) is 0.25 eV lower compared with RS LiCl (2.54 Å apart). Here, it is likely that this strengthening in bondings for WZ structure outweighs the increase in Madelung constant for RS structure. This dependence of binding energy on the interatomic distance for ionic Li—Cl is compared with covalent H—Cl of the same group in Fig. 2D, revealing the typical long-range feature of Coulomb interactions compared with brittle covalent bondings. Note that, upon an elongation of 0.5 Å from the ground state, the binding energy of Li—Cl and H—Cl are 0.52 and 1.50 eV, respectively, higher. It is likely that the switching barriers of ionic WZ structures can be much lower compared with covalent ones when their ion displacements are similar.

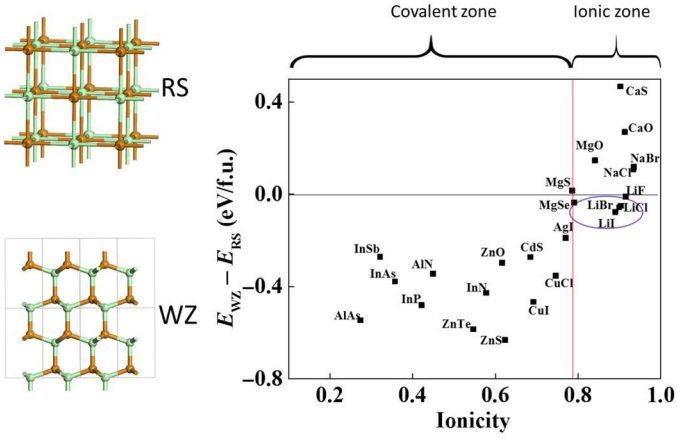

Fig. 1. The geometric structures of RS and WZ structures and the dependence of their energy difference on Philips ionicity for a series of binary compounds. RS, rock salt; WZ, wurtzite.

Now, we explore the possible pathway to reverse the polarizations stemming from the breaking of inversion symmetry by the configuration of covalent-like sp^3 bondings in WZ structures. The ferroelectric switching pathway of WZ LiCl calculated using nudged elastic band method is displayed in Fig. 3A, which indicates a low barrier around 0.04 eV/f.u., much reduced compared with the barriers over 0.25 eV/f.u. for WZ ZnO (*4*) and AgI (*6*). The intermediate state (i.e., paraelectric phase) is shown in Fig. 3B, and its instability is revealed by the phonon dispersion, where the imaginary soft mode is associated with ferroelectric transition. It is composed of planar hexagonal LiCl layers and only 0.04 eV/f.u. higher in energy compared with the ferroelectric ground state. Here, the shortest interlayer Li—Cl distance (2.65 Å) is only slightly longer compared with intralayer Li—Cl bonds (2.41 Å), so each Li and Cl atoms can be deemed as penta-coordinated. For a covalent WZ system with directional and saturated sp^3 bondings, a high energy cost will be required to transform to this intermediate state with altering bonding angles and coordination numbers. In contrast, this transition in lithium halides is much easier with nondirectional and nonsaturated ionic bondings, where the switching process is smoother and refrained from abrupt bond breaking due to the long-range feature of Coulomb interactions. For LiBr, LiI, MgS, and MgSe that are relatively more covalent with lower ionicity, the relative stability of WZ structures and their switching barriers shown in Fig. 3B are enhanced, while this barrier for WZ LiF is reduced to 12 meV/f.u. As summarized in Table 2, the polarization of those WZ structures are comparable or even much larger compared with most perovskite ferroelectrics such as $BaTiO_3$ (~0.26 C/m^2).

The features of ionic bondings that facilitate structural deformation may also reduce the barrier of phase transition, noting that the RS state is only 0.05 eV/f.u. higher in energy compared with WZ for LiCl in Fig. 1. Our calculations of the phase transformation pathway in Fig. 4 also reveal a moderate barrier around 0.08 eV/f.u. for WZ-RS transition and a low barrier around 0.03 eV/f.u. for RS-WZ transition. The intermediate structure indicates the continuous transition between buckled honeycomb lattice for WZ state and planar square lattice for RS state from the overview of $-xy$ plane. Considering the large difference in lattice constants (a = 6.79 Å, b = 3.92 Å, c = 6.29 Å for WZ and $a = b = c$ = 5.15 Å for RS), this high deformation via such a moderate barrier would be incredible without the nondirectional and nonsaturational features of ionic bondings. The phase transition barriers are enhanced for LiI, MgS, and MgSe with

Table 1. The Pauling ion radius (*14*).

	Li^+	Na^+	Mg^{2+}	F^-	Cl^-	Br^-	I^-	S^{2-}	Se^{2-}
r/pm	60	95	65	136	181	195	216	184	198

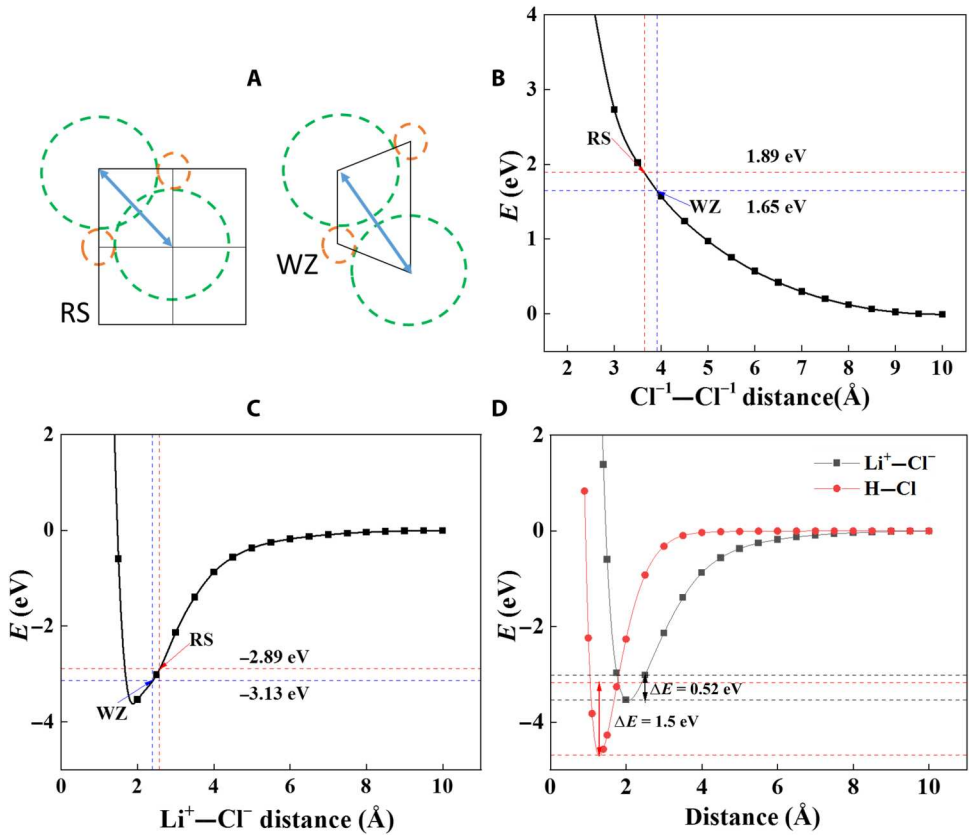

Fig. 2. Analysis of bonding configurations. (**A**) Schematic graphs of the distances between adjacent cations (in orange circles) and anions (in green circles) in RS and WZ structures. (**B**) Distance dependence of the interaction energy between two Cl anions, (**C**) between a Li cation and a Cl anion, and (**D**) a comparison of distance dependence of interaction energy between Li—Cl and H—Cl, with marked energy changes upon an elongation of 0.5 Å from the ground state.

smaller ionicity while much reduced to 0.044 eV/f.u. for LiF, as listed in Table 2.

Despite the higher energy of RS phase compared with WZ phase for those compounds in our calculations, previous experimental reports have shown that some of their RS structures can be more stable at room temperature, although the existence of WZ phases has also been verified (*15*–*19*). The formation of RS phase can be favored by high temperature due to its higher entropy compared with WZ phase that may lead to lower Gibbs free energy, as illustrated in Fig. 5A. Meanwhile, it can also be favored by nanosize because the high polarization of WZ structure will give rise to high electrostatic energy at nanoscale. It is likely that its growth of bulk size will be based on the nanosized nucleation of RS phase. Similarly, in LiCl ultrathin film, the ferroelectric WZ phase may be not preferable due to the depolarization field, where the nonpolar RS phase becomes more favorable below the thickness of 15 layers, as we calculated in Fig. 5B. A substrate with perfect lattice match may facilitate the epitaxial growth of WZ phase, and a case in point is $SnSe_2$ with a honeycomb lattice as the substrate for WZ LiCl(001), where the epitaxial strain is compressive around 1% on monolayer $SnSe_2$ and tensile around 0.1% on the bulk $SnSe_2$. In contrast, it cannot fit any surface of RS phase with a cubic lattice. To our calculations, the binding energy between $SnSe_2$ monolayer substrate and epitaxial seven-layer WZ LiCl thin film turns out to be −1.32 eV for each unit cell of heterointerface shown in Fig. 5C, i.e., the formation energy is lowered by 0.047 eV/f.u. for WZ phase. Therefore, $SnSe_2$ monolayer substrate can further stabilize WZ phase and reduce the critical thickness from around 15 to 7 layers according to the curve in Fig. 5B. Aside from the temperature and film thickness, the relative stability between two phases can also be tuned via doping. For example, considering the preferable structures for CuCl and NaCl, the WZ phase of LiCl can be stabilized

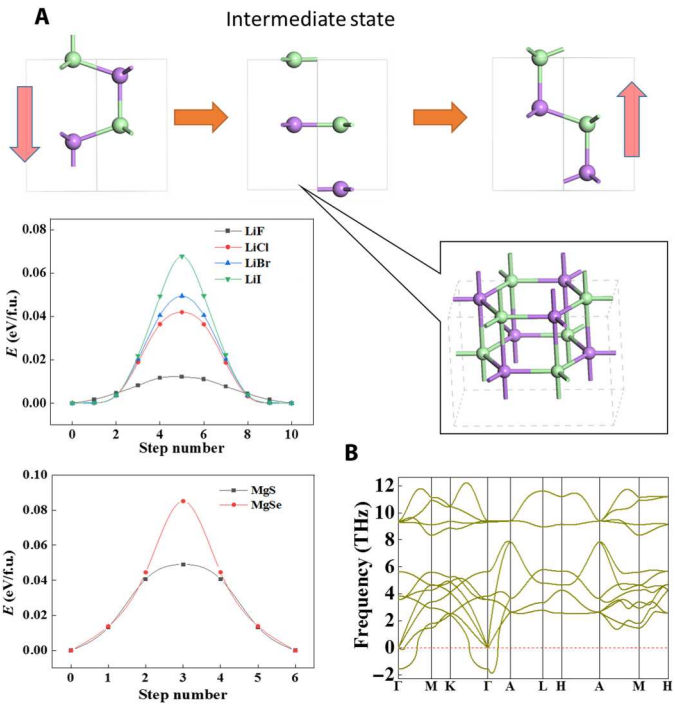

Fig. 3. Ferroelectricity of WZ structures. (**A**) Ferroelectric switching pathways of ionic WZ structures and (**B**) phonon spectrum of intermediate state, where the purple and green spheres, respectively, denote cations and anions, and red arrows denote polarization directions.

Table 2. Philips ionicity (*2*), ferroelectric polarizations, and switching barriers of WZ phase and their transition barriers to RS phase for LiF, LCl, LiBr, LiI, MgS, and MgSe.

	LiF	LiCl	LiBr	LiI	MgS	MgSe
Ionicity	0.915	0.903	0.899	0.890	0.786	0.790
P(C/m^2)	0.42	0.29	0.26	0.22	0.54	0.50
Switching barrier (eV/f.u.)	0.012	0.042	0.049	0.068	0.049	0.085
Transition barrier (eV/f.u.)	0.044	0.079	0.074	0.095	0.101	0.136

by doping Cu ions, while its RS phase is favored by doping Na ions. Because the RS state is tuned to be slightly more stable than WZ state, nonpolar RS phase can be driven to polar WZ phase upon an electric field, giving rise to a polarization–versus–electric field curve similar to antiferroelectric and relaxor ferroelectric capacitors, which may be also used for energy storage (*11*–*13*). Their high performance can be expected, considering the high polarizations of WZ phase stabilized by electric field and their wide bandgaps (up to 13.6 eV) (*20*) against electrical breakdown. Inversely, because of the lower entropy and higher volume per format unit, WZ phase can be transformed to RS phase via pressure or high temperature. It is known that many Li-ion materials such as $Li_2SrNb_2O_7$ exhibit ionic ability (*21*) due to the small size of Li ion, where local

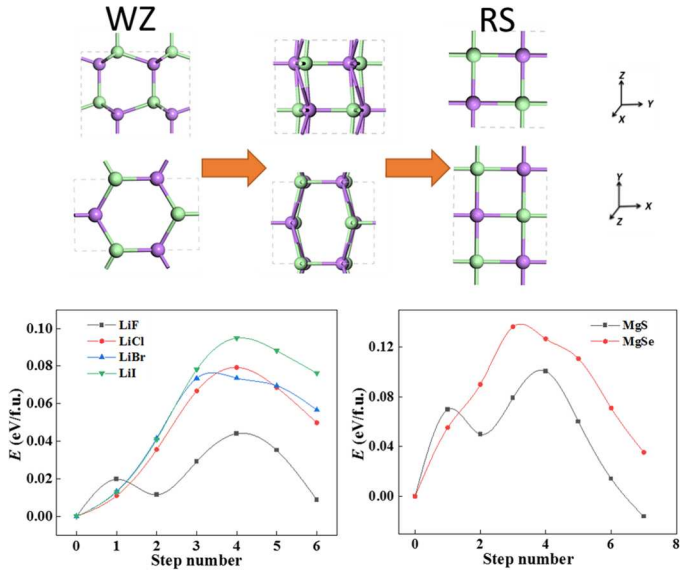

Fig. 4. WZ-RS phase transition pathways.

Li vacancies can be easily induced via applying a voltage. Similarly, in those lithium halides, the charge carriers induced by vacancies may screen part of the ferroelectric polarization, while the migration of vacancies may give rise to "ferroionicity," where even one local vacancy in each conduction channel may induce a high switchable polarization (*22*, *23*).

In summary, we show the abnormal formation of ferroelectric WZ structures and covalent-like sp^3 bondings in highly ionic binary compounds, which contradict with the general principle in the Mooser-Pearson diagram. The high ionicity enables large deformation and long ion displacements with low switching barriers. This ferroelectricity with low-energy consumption in facile binary materials, also with wide bandgaps leading to high breakdown voltages, is highly desirable for nanoelectronic application as nonvolatile random access memories. Meanwhile, their high ionicity also reduces the barrier of phase transition between polar and nonpolar phases, which may facilitate efficient energy storage.

MATERIALS AND METHODS

Our calculations are performed within the framework of density functional theory implemented in the Vienna Ab initio Simulation Package (VASP 5.4) code (*24*, *25*). The projector augmented wave (*26*) potential for the core and the generalized gradient approximation in the Perdew-Burke-Ernzerhof (*27*) form for the exchange-correlation functional are applied. The Monkhorst-Pack k-meshes (*28*) are set to 6 × 6 × 9 in the Brillouin zone, and the electron wave function is expanded on a plane-wave basis set with a cutoff energy of 520 eV. All atoms are relaxed in each optimization cycle until atomic forces on each atom are less than 0.01 eV·Å^{-1}, and the energy variation between subsequent iterations falls below 10^{-6} eV. The Berry phase method is adopted in computing the ferroelectric polarizations (*29*), and a generalized solid-state nudged elastic band method (*30*) is used to calculate the pathway of phase transition.

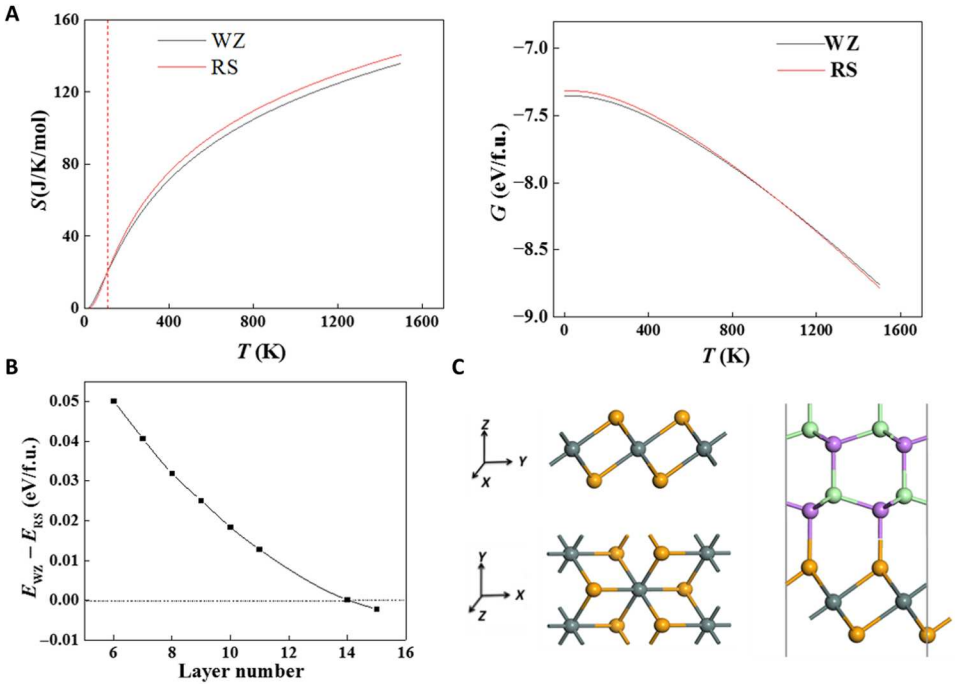

Fig. 5. Tuning the relative stability between WZ and RS phase. (**A**) Entropy and Gibbs free energy (at 1 atm) versus temperature for RS and WZ LiCl. (**B**) Dependence of energy difference between WZ and RS LiCl thin film on layer thickness. (**C**) Geometric structure for $SnSe_2$ monolayer and the interface of thin-film WZ LiCl grown on $SnSe_2$ monolayer.

REFERENCES AND NOTES

1. E. Mooser, W. B. Pearson, On the crystal chemistry of normal valence compounds. *Acta Crystallogr.* **12**, 1015–1022 (1959).
2. J. C. Phillips, Ionicity of the chemical bond in crystals. *Rev. Mod. Phys.* **42**, 317–356 (1970).
3. R. M. Martin, Interatomic forces and ionicity in covalent crystals. *Solid State Commun.* **8**, 799–802 (1970).
4. L. Li, M. Wu, Binary compound bilayer and multilayer with vertical polarizations: Two-dimensional ferroelectrics, multiferroics, and nanogenerators. *ACS Nano* **11**, 6382–6388 (2017).
5. H. Moriwake, A. Konishi, T. Ogawa, K. Fujimura, C. A. J. Fisher, A. Kuwabara, T. Shimizu, S. Yasui, M. Itoh, Ferroelectricity in wurtzite structure simple chalcogenide. *Appl. Phys. Lett.* **104**, 242909 (2014).
6. Y. Gao, M. Wu, X. C. Zeng, Phase transitions and ferroelasticity-multiferroicity in bulk and two-dimensional silver and copper monohalides. *Nanoscale Horiz.* **4**, 1106–1112 (2019).
7. H. Moriwake, R. Yokoi, A. Taguchi, T. Ogawa, C. A. J. Fisher, A. Kuwabara, Y. Sato, T. Shimizu, Y. Hamasaki, H. Takashima, M. Itoh, A computational search for wurtzite-structured ferroelectrics with low coercive voltages. *APL Mater.* **8**, 121102 (2020).
8. S. Fichtner, N. Wolff, F. Lofink, L. Kienle, B. Wagner, AlScN: A III-V semiconductor based ferroelectric. *J. Appl. Phys.* **125**, 114103 (2019).
9. K. Ferri, S. Bachu, W. Zhu, M. Imperatore, J. Hayden, N. Alem, N. Giebink, S. Trolier-McKinstry, J.-P. Maria, Ferroelectrics everywhere: Ferroelectricity in magnesium substituted zinc oxide thin films. *J. Appl. Phys.* **130**, 044101 (2021).
10. A. I. Khan, A. Keshavarzi, S. Datta, The future of ferroelectric field-effect transistor technology. *Nat. Electron.* **3**, 588–597 (2020).
11. B. Xu, J. Iniguez, L. Bellaiche, Designing lead-free antiferroelectrics for energy storage. *Nat. Commun.* **8**, 15682 (2017).
12. H. Pan, S. Lan, S. Xu, Q. Zhang, H. Yao, Y. Liu, F. Meng, E.-J. Guo, L. Gu, D. Yi, X. Renshaw Wang, H. Huang, J. L. MacManus-Driscoll, L.-Q. Chen, K.-J. Jin, C.-W. Nan, Y.-H. Lin, Ultrahigh energy storage in superparaelectric relaxor ferroelectrics. *Science* **374**, 100–104 (2021).
13. L. Chen, S. Deng, H. Liu, J. Wu, H. Qi, J. Chen, Giant energy-storage density with ultrahigh efficiency in lead-free relaxors via high-entropy design. *Nat. Commun.* **13**, 3089 (2022).
14. L. Pauling, The sizes of ions and the structure of ionic crystals. *J. Am. Chem. Soc.* **49**, 765–790 (1927).
15. A. Bach, D. Fischer, M. Jansen, Synthesis of a new modification of lithium chloride confirming theoretical predictions. *Z. Anorg. Allg. Chem.* **635**, 2406–2409 (2009).
16. D. Fischer, A. Mueller, M. Jansen, Is there a wurtzite-modification of lithium bromide? — Studies on the system LiBr/LiI. *ChemInform* **36**, (2005).
17. Y. H. Lai, Q. L. He, W. Y. Cheung, S. K. Lok, K. S. Wong, S. K. Ho, K. W. Tam, I. K. Sou, Molecular beam epitaxy-grown wurtzite MgS thin films for solar-blind ultra-violet detection. *Appl. Phys. Lett.* **102**, 171104 (2013).
18. Y. Liebold-Ribeiro, D. Fischer, M. Jansen, Experimental substantiation of the "energy landscape concept" for solids: Synthesis of a new modification of LiBr. *Angew. Chem. Int. Ed.* **47**, 4428–4431 (2008).
19. F. Jiang, Q. Liao, G. Fan, C. Xiong, X. Peng, C. Pan, N. Liu, MOCVD growth of MgSe thin films on GaAs substrates. *J. Cryst. Growth* **183**, 289–293 (1998).
20. F. C. Brown, C. Gähwiller, H. Fujita, A. B. Kunz, W. Scheifley, N. Carrera, Extreme-ultraviolet spectra of ionic crystals. *Phys. Rev. B Condens. Matter* **2**, 2126–2138 (1970).
21. X. Xu, F.-T. Huang, K. Du, S.-W. Cheong, Multifunctionality of Li2SrNb2O7: Memristivity, tunable rectification, ferroelasticity, and ferroelectricity. *Adv. Mater.* **34**, 2206022 (2022).
22. A. N. Morozovska, E. A. Eliseev, N. V. Morozovsky, S. V. Kalinin, Ferroionic states in ferroelectric thin films. *Phys. Rev. B Condens. Matter* **95**, 195413 (2017).
23. X. Wang, Y. Ren, M. Wu, Unconventional ferroelectricity with quantized polarizations in ionic conductors: High-throughput screening. *J. Phys. Chem. Lett.* **13**, 9552–9557 (2022).
24. G. Kresse, J. Furthmüller, Efficiency of ab-initio total energy calculations for metals and semiconductors using a plane-wave basis set. *Comp. Mater. Sci.* **6**, 15–50 (1996).
25. G. Kresse, J. Furthmüller, Efficient iterative schemes for ab initio total-energy calculations using a plane-wave basis set. *Phys. Rev. B Condens. Matter* **54**, 11169–11186 (1996).
26. P. E. Blöchl, Projector augmented-wave method. *Phys. Rev. B Condens. Matter* **50**, 17953–17979 (1994).
27. J. P. Perdew, K. Burke, M. Ernzerhof, Generalized gradient approximation made simple. *Phys. Rev. Lett.* **77**, 3865–3868 (1996).
28. H. J. Monkhorst, J. D. Pack, Special points for Brillouin-zone integrations. *Phys. Rev. B Condens. Matter* **13**, 5188–5192 (1976).
29. R. D. King-Smith, D. Vanderbilt, Theory of polarization of crystalline solids. *Phys. Rev. B Condens. Matter* **47**, 1651–1654 (1993).
30. G. Henkelman, B. P. Uberuaga, H. Jónsson, A climbing image nudged elastic band method for finding saddle points and minimum energy paths. *J.Chem.Phys.* **113**, 9901–9904 (2000).

Acknowledgments: We thank Shanghai Supercomputer Center for providing computing resource. **Funding:** This work is supported by National Natural Science Foundation of China

(no. 22073034). **Author contributions:** M.W. conceived the idea. Y.D. performed the calculations and analyzed the data. Y.D. and M.W. wrote the manuscript. **Competing interests:** The authors declare that they have no competing interests. **Data and materials availability:** All data needed to evaluate the conclusions are present in the paper.

Submitted 17 November 2022
Accepted 21 December 2022
Published 20 January 2023
10.1126/sciadv.adf8706